Supporting Information:

Two different structures of the oxygen-evolving complex in the same polypeptide frameworks of photosystem II

Ayako Tanaka[†], Yoshimasa Fukushima[‡], Nobuo Kamiya[†, ‡, *]

[†]Department of Chemistry, Graduate School of Science, Osaka City University, 3-3-138 Sugimoto, Sumiyoshi, Osaka 558-8585, Japan; [‡]The OCU Advanced Research Institute for Natural Science and Technology (OCARINA), Osaka City University, 3-3-138 Sugimoto, Sumiyoshi, Osaka 558-8585, Japan.

[*] Corresponding author: nkamiya@sci.osaka-cu.ac.jp

Definition of PSII subunits and two monomers in the crystallographic asymmetric unit

Photosystem II (PSII) exists in the asymmetric unit of the crystal as a homodimer, and each monomer is composed of 19 or 20 protein subunits, as shown in Figure S1, where the left and right sides are defined as the A- and B-monomer, respectively. Four of the subunits are major hydrophobic trans-membrane subunits (PsbA, PsbB, PsbC, and PsbD), conventionally denoted as D1, CP47, CP43, and D2, respectively. Twelve or thirteen are minor trans-membrane subunits, and the remaining three are extrinsic hydrophilic subunits (PsbO, PsbU, and PsbV). The A- and B-monomers in the LowDose-1 (at 0.03 MGy, PDB-ID; 5B5E) and LowDose-2 (at 0.12 MGy, 5B66) structures are located in the crystal lattice having the centers of gravity (COG) at (X, Y, Z) coordinates of (19, 43, 50) and (7, -19, 5) in Å units, respectively. Because COGs of the two monomers in Native_0.43MGy (3WU2)[1], XFEL-1 (4UB6)[2], and XFEL-2 (4UB8)[2] are different from those of LowDose-1 and LowDose-2, the structures should be translated by X-ray crystallographic rotation or translation of the lattice origin to superpose onto LowDose-1 and LowDose-2. The Native_0.43MGy and XFEL-2 structures are related by the two-fold axes rotation around the crystallographic *c*-axis and *b*-axis, respectively. The XFEL-1 structure is related by the one-unit translations along the *b*- and *c*-axes. Although the COGs of the two monomers in the five structures are different, the monomers with the names of capital letters in the PDB coordinate files correspond to the A-monomer, and those with the names of small letters to the B-monomer.

As indicated by red ovals in Figure S1, the D1 and D2 subunits of PSII are surrounded by CP47 and CP43 in the trans-membrane region and by the three extrinsic subunits in the hydrophilic region. Interactions between the subunits result in D1 and D2 being the most stable subunits in PSII. D1 and D2 are highly conserved in order to hold the reaction center, P680, the pigments for electron transfer, as well as the OEC[1]. One PSII monomer binds two electron-acceptor plastoquinones (Q_A and Q_B). The averaged temperature factors of Q_A for both the A- and B-monomers in the LowDose-1 structure at 0.03 MGy were small, at 22 $Å^2$, but those of Q_B were very high, at 62 and 66 $Å^2$, indicating that Q_A is stable and Q_B is flexible. Consistent with the flexibility of Q_B, the temperature factors of the Cα atoms around Q_B at the stromal side of the thylakoid membrane (Ala11-Arg16 and Leu223-Asn267 for D1, Glu11-Ser33 and Leu222-Glu242 for D2) were large, at 37 $Å^2$ in the average.

The oxygen-evolving complex (OEC) of PSII comprises portions of the hydrophobic D1 and CP43 subunits, in addition to four manganese atoms (Mn1-Mn4, see Figures 1(b) and 1(c) of the main text), one calcium atom (Ca), five oxo-bridging oxygen atoms (O1-O5), and four ligand-water molecules (W1-W4). W1-W4 can also be hydroxide ions. The OEC is directly ligated by the C-terminal carboxylate group of the D1 subunit (D1-Ala344), two aspartates (D1-Asp170, D1-Asp342), two glutamates (D1-Glu189, D1-Glu333), one histidine (D1-His332), and one glutamate residue from the CP43 subunit (CP43-Glu354). Furthermore, the OEC is surrounded by hydrogen bonds with five amino acid residues (CP43-Arg357 facing to O2, O4, D1-Asp170, and D1-Ala344; D1-His337 to O3; D1-Asp61 to W1; D1-Tyr161 and D1-Gln165 to W4) and two water molecules (W5 and W6 facing to O1 and O4, respectively).

Experimental procedures

Purification and crystallization

Purification procedure of PSII was followed by the protocol partially modified from that in the previous literature[1]. Cells of the thermophilic cyanobacterium *Thermosynechococcus vulcanus* were grown in four of 5 L Erlenmeyer flasks at 50 °C. The crude PSII complexes were extracted from the cells using the detergent LDAO. The crude PSII complexes were stabilized with a buffer of 20 mM HEPES-NaOH (pH 7.0), 10 mM $MgCl_2$, 25 %(w/v) glycerol containing 1.0 %(w/v) DDM and were loaded onto Q-Sepharose High Performance column (GE Healthcare Japan) equilibrated with the buffer-A containing 30 mM MES-NaOH (pH 6.0), 170 mM NaCl, 3 mM $CaCl_2$, 5 %(w/v) glycerol, 0.03 %(w/v) DDM. The PSII complexes were eluted by a gradient to 300 mM NaCl with the buffer-A. Eluted PSII-dimer fraction equilibrated in a buffer containing 20 mM MES-NaOH (pH 6.0), 20 mM NaCl, 3 mM $CaCl_2$, 5 %(w/v) glycerol, 0.03 %(w/v) DDM was stored in liquid nitrogen. The oxygen-evolving activity of the PSII-dimer sample was measured in solution and the oxygen-evolving velocity was completely the same for the conditions at the presence and at the absence of DMSO. The PSII-dimer crystals were obtained by the incubation over one week at 12 °C in the crystallization buffer of 20 mM MES-NaOH (pH 6.1), 30 mM NaCl, 11.5 mM $CaCl_2$, 40 mM $MgSO_4$, and 4.8-5.25 %(w/v) PEG1450. To improve the crystal quality, PSII microcrystals were obtained first. The microcrystals were dissolved in the crystallization buffer again under the dim green light and the solution was stored over for one week in the dark condition for the second crystallization step. For the dehydration procedure, the crystals obtained were moved under the dim green light into

the cryo-buffer of 50 μl containing 20 mM MES-NaOH (pH 6.1), 20 mM NaCl, 10 mM $CaCl_2$ and 10 %(w/v) PEG3000. After 30 min of incubation at 12 °C, half of the buffer volume was replaced with a new buffer containing PEG3000 of 1.1 % higher concentration and 2.8 %(w/v) DMSO. This procedure was repeated every 30 min until the concentrations of PEG3000 and DMSO reached to 20 %(w/v) and 25 %(w/v), respectively. The pH value of the solution increased gradually to pH 6.3 in parallel with the increment of PEG3000 and DMSO concentrations. Finally, the crystals were incubated in the buffer of the last condition (pH was further adjusted at 6.6) for 17 h in the dark at 12 °C and were flash-cooled in a nitrogen gas stream at 100 K and then stored in liquid nitrogen.

Measurements of Mn K-absorption edge profiles of PSII crystals

Mn K-absorption edge profiles of PSII crystals were measured at a bending-magnet beamline, BL26B1 of SPring-8 using the equipment installed for phase determination of reflections by the multi-wavelength anomalous dispersion method. One Si-PIN X-ray detector (XR-100CR) was placed for counting fluorescence X-ray photons from sample crystals in the horizontal plane with an angle of 90° from the incident X-ray beam. PSII crystals were mounted at 100 K on a χ-type attachment (χ=25°) set on the crystal rotation axis (ϕ-axis). Angles between the incident X-ray beam and crystal surface planes were around 115°. The region of Mn K-absorption edge was measured in the wavelength range from 1.8893 Å (corresponding energy, 6562.3 eV) to 1.8974 Å (6534.3 eV) with a step of 0.0003 Å. In order to reduce X-ray dose to 0.01 MGy, the measurements were repeated 32 times using 12 PSII crystals sliding positions of each sample toward the ϕ-axis. As a reference of X-ray wavelength (or energy) at BL26B1, similar measurements were performed 12 times for a solution sample of 10 mM $MnCl_2$. All fluorescence intensities were integrated and the values normalized by the incident beam intensities were scaled at 1.8971 Å to zero and at 1.8902 Å to unity as shown in Figure S2.

Diffraction intensity measurements and structure analyses

We used highly isomorphous crystals of PSII in order to reduce the X-ray doses in data collections. The crystals were mounted on the beamline equipment at a bending-magnet beamline, BL38B1, and an udulater beamline, BL44XU of SPring-8, Japan, under the near-infrared LED light of wavelength around 810 nm. A part of the reflections in the reciprocal diffraction space were measured independently in the dark from each of 10 isomorphous crystals at BL38B1 (the LowDose-1 dataset at 0.03 MGy

in Table S1), and from each of three crystals at BL44XU (the LowDose-2 dataset at 0.12 MGy). The incident X-ray beam positions on the crystals were shifted along the crystal rotation ϕ-axis without overlapping of the beam area after that the X-ray doses reached to the indicated values. The total measurement points on the crystals were 46 and 42 for the LowDose-1 and LowDose-2 datasets, respectively. All reflection intensities were integrated using *XDS*[3], and scaled and merged using *SCALA*[4] in the *CCP4* program suite. The averaged dose value of 0.03 MGy, calculated using *RADDOSE*[5], corresponded to fewer than 1 % of the OECs being reduced to Mn(II)[6], which is negligible. The 0.12 MGy dose corresponded to 3.5 % of the OECs being reduced to Mn(II). The resolutions were improved from the 1.9 Å of the Native_0.43MGy dataset reported previously: 1.87 and 1.85 Å for the LowDose-1 and LowDose-2 datasets, respectively. The averaged redundancies for measuring unique reflections were large, at 11.3 and 15.5, and R_{pim} values[7], a reliability factor for taking redundancies into account, were reasonably small at less than 40 % at the highest resolution shells. Thus the two datasets were expected to be highly reliable.

Initial structures were obtained by the molecular replacement method with *MOLREP*[8]. The search model used was a poly-Ala structure (Gly remained as it was) produced from the Native_0.43MGy structure (3WU2)[1], in which amino acid residues with relatively high temperature factors were omitted. Restrained least-squares refinement was started from a resolution of 2.8 Å to the highest resolutions using *REFMAC5*[9]. When clear electron density distributions were found on $2|F_o| - |F_c|$ maps at the 1.0-sigma level and $|F_o| - |F_c|$ difference Fourier maps at the 3.0-sigma level, structure models were constructed using *COOT*[10]. To minimize model biases, the structure models were verified by comparing the $2|F_o| - |F_c|$ maps with composite omit maps generated by *CNS*[11] at several stages of refinement. OEC models were constructed at the final stage of refinement. Four Mn atoms and one Ca atom were assigned from the $2|F_o| - |F_c|$ maps. Five oxo-bridging oxygen atoms were identified from the $|F_o| - |F_c|$ maps calculated after one *REFMAC5* refinement. The restrained structural information for the OECs of the A- and B-monomers in the asymmetric unit were individually defined and used for further refinement cycles. The final statistics of the restrained least-squares refinement were listed in Table S2. Graphic representations of the structures were obtained using *PyMol*[12].

Error estimation for comparisons of atomic distances

Atomic distances in the OECs are compared in Figures S5 and S6 for the LowDose-1 and LowDose-2 structures obtained in this study and Native_0.43MGy[1].

Numerical values are listed in Tables S3 and S4, as well as for the two structures resolved using XFEL[2] (XFEL-1 and XFEL-2). Error estimations are generally very important for comparing atomic distances. The diffraction-component precision index (DPI)[13] is given as a root-mean-squares deviation (r. m. s. d.) of atomic coordinates from the restrained least-squares refinement. The DPI values are calculated based on the assumption that all atoms in a structure have the same temperature factors (averaged temperature factor, B_{av}). For the LowDose-1 and LowDose-2 structures in this study and for Native_0.43MGy, the B_{av} values were all close to 34 Å^2. The corresponding DPI values were calculated to be 0.12, 0.11, and 0.11 Å, for the LowDose-1 and LowDose-2, and Native_0.43MGy structures, respectively, and the error estimations for atomic distances were all around 0.16 Å. On the other hand, the individual temperature factors of atoms in the OEC were around 20 Å^2 (see Table S5), which is significantly smaller than the B_{av} values. Because the smaller temperature factors corresponded to smaller deviations in atomic distance, the error value of the 0.16 Å was over-estimated for the OEC. To obtain another estimation of the error, we calculated an r. m. s. d. value of 0.05 Å from superimpositions of the A- or B-monomers in the LowDose-1 and LowDose-2 structures using parts of the D1 (Phe17-Ser222 and Ser268-A344) and D2 (Gly34-Thr221 and Thr243-Leu352) subunits. These parts were composed of Cα atoms with the smallest averaged temperature factor, and were thus expected to be the most stable in PSII. We adopted the value of 0.05 Å as an under-estimated standard deviation for atomic distances and assumed 0.1 Å as the error value, which is in the middle of the over-estimated 0.16 Å and the under-estimated 0.05 Å.

Table S1. X-ray diffraction intensity measurements and data statistics.

Data set	LowDose-1	LowDose-2
Beamline	BL38B1, SPring-8	BL44XU, SPring-8
Wavelength (Å)	0.9	0.9
Beamline flux (phs s^{-1})	3.74×10^{10}	3.01×10^{12}
Beam size (μm^2)	80×160	50×55
Al attenuator (cm)	0.07	0.08
Incident flux (phs s^{-1})	5.66×10^{9}	3.36×10^{11}
Averaged dose (MGy)	0.03	0.12
Used crystals	10	3
Measurement points	46	42
Space group	$P2_12_12_1$	$P2_12_12_1$
Unit cell *a, b, c* (Å)	121.4, 228.2, 286.4	121.5, 228.2, 286.4
Resolution (Å)	49.0-1.87(1.97-1.87)	49.0-1.85(1.95-1.85)
Measured reflections	7,345,201(1,067,583)	10,409,183(1,500,378)
Unique reflections	649,016(94,243)	671,082(97,435)
R_{merge} (%)(i)	13.1(127)	11.8(150)
$\langle I \rangle / \langle \sigma(I) \rangle$	17.2(2.0)	20.5(1.9)
Completeness (%)	99.9(100)	100(100)
Redundancy	11.3(11.3)	15.5(15.4)
R_{pim} (%)(ii)	4.0(38.6)	3.1(39.4)
CC(1/2)(iii)	99.8(73.3)	99.9(79.9)

Numbers in parentheses are for the highest resolution shell.

(i) Linear merging R-value.

$$R_{merge} = \frac{\sum_{hkl}\sum_{i=1}^{N}\left|I_i(hkl) - \overline{I(hkl)}\right|}{\sum_{hkl}\sum_{i=1}^{N} I_i(hkl)}$$

$I_i(hkl)$ is an integrated intensity of one reflection. The suffix *i* is for equivalent reflections and *N* is their number. $\overline{I(hkl)}$ is an average for one unique reflection and the suffix *hkl* means unique reflections.

(ii) Precision-indicating merging R-value.

$$R_{pim} = \frac{\sum_{hkl}\left(\frac{1}{N-1}\right)^{1/2}\sum_{i=1}^{N}\left|I_i(hkl)-\overline{I(hkl)}\right|}{\sum_{hkl}\sum_{j=1}^{N}I_i(hkl)}$$

(iii) A correlation coefficient of integrated intensities between two half datasets randomly divided.

Table S2. Restrained least-squares refinement statistics.

Data set	LowDose-1	LowDose-2
Resolution (Å)	50 – 1.87	20 – 1.85
R / R_{free}	0.17 / 0.21	0.16 / 0.20
DPI (Å)	0.12	0.11
No. of chains	38	38
No. of residues	5383	5234
No. of water molecules	3625	3925
No. of ligand molecules	366	347
Averaged B-factor (Å^2)	33.6	35.3
R.M.S. deviations		
Bond lengths (Å)	0.017	0.016
Bond angles (deg)	2.38	2.32
Ramachandran plot (%)		
Favoured region	96.9	97.1
Allowed region	2.69	2.53
Outlier region	0.45	0.37

Table S3. Atomic distances (Å) between different pairs of metal ions in the oxygen-evolving complex.

	LowDose-1	LowDose-2	*Native_0.43MGy[1]	XFEL-1[2]	XFEL-2[2]
	5B5E	5B66	3WU2	4UB6	4UB8
Mn1-Mn2	2.74, 2.65	2.73, 2.72	2.87, 2.76	2.61, 2.67	2.74, 2.68
Mn1-Mn3	3.22, 3.22	3.22, 3.24	3.28, 3.29	3.18, 3.24	3.27, 3.10
Mn1-Mn4	4.91, 4.88	4.92, 4.89	4.99, 4.92	4.97, 4.95	4.97, 4.89
Mn2-Mn3	2.76, 2.77	2.78, 2.82	2.88, 2.92	2.67, 2.70	2.73, 2.71
Mn2-Mn4	5.22, 5.17	5.25, 5.21	5.44, 5.38	5.18, 5.17	5.21, 5.27
Mn3-Mn4	2.82, 2.75	2.85, 2.77	2.97, 2.89	2.83, 2.86	2.88, 2.91
Ca-Mn1	3.50, 3.51	3.51, 3.48	3.55, 3.49	3.45, 3.51	3.49, 3.43
Ca-Mn2	3.35, 3.29	3.34, 3.30	3.39, 3.30	3.29, 3.35	3.33, 3.32
Ca-Mn3	3.39, 3.40	3.40, 3.39	3.42, 3.41	3.39, 3.47	3.41, 3.33
Ca-Mn4	3.75, 3.78	3.77, 3.74	3.79, 3.80	3.86, 3.76	3.71, 3.76
Averaged difference**	—	0.013	0.082	0.002	0.003

*The name is combined with the averaged X-ray dose. Two values in each frame are corresponding to A- and B-monomers. **The averaged difference of atomic distances, calculated using the LowDose-1 structure as the standard.

Table S4. Bond lengths (Å) in the oxygen-evolving complex.

Atom	Ligand	LowDose-1	LowDose-2	*Native_0.43MGy[1]	XFEL-1[2]	XFEL-2[2]
		5B5E	5B66	3WU2	4UB6	4UB8
Mn1	O1	1.87, 1.65	1.75, 1.70	1.85, 1.80	1.85, 1.80	1.81, 1.73
	NE2-H332	2.03, 2.01	2.01, 2.07	2.09, 2.15	2.08, 2.11	2.13, 2.16
	O3	1.76, 1.91	1.85, 1.92	1.84, 1.93	1.94, 1.93	1.80, 1.80
	OE2-E189	1.88, 1.84	1.88, 1.85	1.87, 1.71	1.78, 1.76	1.81, 1.81
	O5	2.74, 2.77	2.71, 2.82	2.65, 2.66	2.70, 2.72	2.70, 2.69
	OD2-D342	2.16, 2.20	2.13, 2.17	2.22, 2.28	2.16, 2.19	2.26, 2.25
	Averaged difference**	—	0.003	0.019	0.017	0.011
Mn2	O1	1.83, 1.95	1.93, 1.96	2.08, 2.07	1.83, 1.72	1.88, 1.83
	OE1-E354	2.02, 2.07	2.05, 2.11	2.09, 2.16	2.12, 2.07	2.10, 2.09
	O2	1.93, 1.83	1.99, 1.84	2.16, 1.96	1.90, 1.74	1.83, 1.83
	OD1-D342	2.17, 2.08	2.11, 2.03	2.15, 2.04	2.14, 2.19	2.16, 2.15
	O3	2.06, 1.89	1.98, 1.94	2.13, 2.02	1.95, 2.06	2.01, 2.07
	OXT-A344	1.96, 1.94	1.99, 1.93	1.97, 1.85	1.92, 1.85	1.97, 1.86
	Averaged difference**	—	0.011	0.079	-0.020	0.004
Mn3	O2	1.81, 1.82	1.81, 1.90	1.93, 1.91	1.78, 1.81	2.00, 2.00
	OE1-E333	1.99, 1.99	1.91, 1.95	2.02, 1.94	2.03, 2.08	2.04, 2.08
	O3	2.27, 1.96	2.18, 1.95	2.24, 1.86	2.08, 1.99	2.14, 2.02
	O4	1.87, 1.95	1.88, 1.96	2.05, 2.06	1.91, 1.92	1.89, 1.88
	O5	2.09, 2.07	2.14, 2.02	2.28, 2.25	2.17, 2.02	2.32, 2.30
	OE2-E354	2.12, 2.18	2.17, 2.16	2.21, 2.17	2.12, 2.12	2.16, 2.12
	Averaged difference**	—	-0.008	0.067	-0.008	0.069
Mn4	O4	1.87, 2.07	1.84, 2.10	2.09, 2.05	1.94, 2.04	2.05, 2.03
	W1	2.19, 2.10	2.19, 2.10	2.27, 2.17	2.34, 2.15	2.26, 2.24
	O5	2.24, 2.17	2.28, 2.12	2.43, 2.34	2.32, 2.30	2.38, 2.33
	W2	2.04, 2.17	2.13, 2.15	2.12, 2.20	2.14, 1.97	2.14, 2.14
	OD1-D170	2.00, 2.07	2.04, 2.08	2.06, 2.11	2.05, 2.08	2.00, 2.00
	OE2-E333	2.06, 2.05	2.05, 2.10	2.17, 2.13	2.07, 2.10	2.06, 2.10
	Averaged difference**	—	0.013	0.093	0.039	0.058

*The name is combined with the averaged X-ray dose. Two values in each frame are corresponding to A- and B-monomers. **The averaged difference of atomic distances, calculated using the LowDose-1 structure as the standard.

Table S4. Bond lengths (Å) in the oxygen-evolving complex (continued).

Atom	Ligand	LowDose-1	LowDose-2	*Native_0.43MGy[1]	XFEL-1[2]	XFEL-2[2]
		5B5E	5B66	3WU2	4UB6	4UB8
Ca	O1	2.39, 2.65	2.43, 2.60	2.39, 2.44	2.57, 2.61	2.64, 2.61
	O2	2.53, 2.56	2.51, 2.56	2.53, 2.48	2.67, 2.58	2.73, 2.69
	O5	2.44, 2.61	2.50, 2.46	2.43, 2.57	2.59, 2.60	2.43, 2.52
	W3	2.33, 2.51	2.36, 2.47	2.34, 2.42	2.61, 2.60	2.59, 2.59
	O-A344	2.52, 2.54	2.51, 2.56	2.55, 2.43	2.41, 2.43	2.43, 2.43
	W4	2.43, 2.46	2.37, 2.45	2.46, 2.40	2.51, 2.49	2.44, 2.42
	OD2-D170	2.40, 2.31	2.42, 2.36	2.42, 2.36	2.28, 2.46	2.34, 2.34
	Averaged difference**	—	-0.009	-0.033	0.052	0.037
O1	W5	2.76, 2.74	2.75, 2.69	2.66, 2.71	2.54, 2.43	2.60, 2.45
	Averaged difference**	—	-0.030	-0.065	-0.265	-0.225
O2	NH2-R357	2.95, 3.09	2.93, 3.03	2.79, 2.98	3.01, 3.28	2.95, 3.04
	Averaged difference**	—	-0.040	-0.135	0.125	-0.025
O3	NE2-H337	2.46, 2.75	2.48, 2.74	2.46, 2.80	2.60, 2.65	2.65, 2.67
	Averaged difference**	—	0.005	0.025	0.020	0.055
O4	W6	2.66, 2.44	2.71, 2.45	2.58, 2.43	2.59, 2.59	2.61, 2.69
	Averaged difference**	—	0.030	-0.045	0.040	0.100
	NH2-R357	3.15, 2.88	3.16, 2.90	3.00, 3.16	3.03, 2.93	2.93, 3.06
	Averaged difference**	—	0.015	0.065	-0.035	-0.020
NH1-R357	OD2-D170	3.04, 3.31	3.04, 3.24	3.16, 3.25	3.47, 3.35	3.29, 3.58
	Averaged difference**	—	-0.035	0.030	0.235	0.260
	O-A344	2.84, 3.12	2.82, 3.18	2.89, 3.18	3.46, 3.33	3.23, 3.27
	Averaged difference**	—	0.020	0.055	0.415	0.270
OE1-E189	W4	2.92, 3.06	2.97, 2.96	2.95, 2.97	3.11, 2.91	2.99, 3.14
	Averaged difference**	—	-0.025	-0.030	0.020	0.075

*The name is combined with the averaged X-ray dose. Two values in each frame are corresponding to A- and B-monomers. **The averaged difference of atomic distances, calculated using the LowDose-1 structure as the standard.

Table S5. Temperature factors of atoms (Å^2) in the oxygen-evolving complex.

Atom	LowDose-1	LowDose-2	*Native_0.43MGy[1]	XFEL-1[2]	XFEL-2[2]
	5B5E	5B66	3WU2	4UB6	4UB8
Mn1	19, 21	21, 23	22, 26	20, 25	21, 27
Mn2	20, 23	22, 24	23, 26	22, 23	23, 25
Mn3	20, 22	22, 23	23, 25	20, 22	22, 25
Mn4	22, 23	24, 25	27, 29	22, 23	24, 25
Ca	23, 24	25, 26	25, 28	28, 34	32, 37
O1	19, 21	20, 21	22, 23	21, 20	28, 24
O2	22, 23	23, 23	26, 28	24, 20	24, 23
O3	20, 24	21, 23	23, 29	25, 24	21, 36
O4	24, 22	23, 24	28, 27	20, 19	24, 20
O5	20, 23	23, 26	24, 26	15, 19	17, 20
W1	17, 18	21, 21	23, 26	19, 30	20, 21
W2	25, 20	26, 24	28, 30	16, 18	30, 27
W3	24, 20	23, 24	26, 29	18, 39	25, 37
W4	21, 23	26, 26	27, 29	40, 39	42, 46
W5	27, 27	29, 32	38, 33	30, 47	48, 46
W6	20, 20	22, 22	24, 26	16, 21	20, 20
OD1-D170	21, 21	23, 22	26, 28	21, 26	25, 25
OD2-D170	23, 23	25,26	25, 27	28, 38	34, 39
OE1-E189	24, 25	26, 25	27, 30	30, 28	30, 31
OE2-E189	19, 20	22, 24	25, 24	16, 26	23, 31
NE2-H332	17, 22	20, 24	19, 26	20, 22	17, 27
OE1-E333	18, 22	22, 23	24, 29	19, 21	22, 32
OE2-E333	16, 20	21, 22	22, 25	22, 21	24, 23
NE2-H337	20, 19	21, 24	22, 29	19, 20	24, 21
OD1-D342	20, 18	24, 21	20, 25	17, 20	21, 24
OD2-D342	20, 19	22, 21	24, 25	18, 22	17, 23
O-A344	23, 25	28, 29	29, 30	29, 22	31, 29
OXT-A344	22, 27	23, 28	25, 33	28, 20	22, 22

*The name is combined with the averaged X-ray dose. Two values in each frame are corresponding to A- and B-monomers.

Table S5. Temperature factors of atoms (Å^2) in the oxygen-evolving complex (continued).

Atom	LowDose-1	LowDose-2	*Native_0.43MGy[1]	XFEL-1[2]	XFEL-2[2]
	5B5E	5B66	3WU2	4UB6	4UB8
OE1-E354	21, 25	24, 24	23, 26	24, 28	23, 28
OE2-E354	19, 22	25, 22	23, 25	21, 23	21, 24
NH1-R357	19, 23	21, 22	24, 33	20, 23	21, 24
NH2-R357	17, 20	21, 25	28, 33	27, 26	26, 27

*The name is combined with the averaged X-ray dose. Two values in each frame are corresponding to A- and B-monomers.

Figure legends

Fig. S1. Overall structure of the PSII dimer from *Thermosynechococcus vulcanus* viewed (a) from the stromal side of the thylakoid membrane and (b) parallel to the membrane surface. The protein subunits are colored individually and their names are depicted for the A-monomer on the left side; the B-monomer is on the right side. The major hydrophobic and hydrophilic subunits are represented with large characters. Ovals in red indicate the D1(PsbA) and D2(PsbD) subunits in the A-monomer. The A- and B-monomers are composed of the PSII subunits with capital and small letters in the PDB files of PSII, respectively.

Fig. S2. Mn K-absorption edge profile of PSII crystal (closed square). The edge profile of 10 mM $MnCl_2$ solution (open square) was measured as a reference of X-ray energy of a bending-magnet beamline, BL26B1 of SPring-8.

Fig. S3. A stereodrawing of the OEC model in the B-monomer of LowDose-1 at a dose of 0.03 MGy. $2|F_o| - |F_c|$ electron density maps are represented by blue mesh at the 1.0-sigma level. $|F_o| - |F_c|$ difference Fourier maps are drawn in green at the 3.5-sigma level. A peak was observed in the $|F_o| - |F_c|$ map near the Cα atom, whereas this peak was absent in the corresponding map for the A-monomer. This was a further indication that the OECs in the A- and B-monomers were different.

Fig. S4. Electron density maps and structure models around the OECs of LowDose-1 at a dose of 0.03 MGy, represented as the developments of cubes, (a) for the A-monomer and (b) for the B-monomer. Each of maps and models is drown as a thin slice. $2|F_o| - |F_c|$ electron density maps are represented by blue mesh at the 1.0-sigma level. $|F_o| - |F_c|$ difference Fourier maps are drawn in green at the 3.0-sigma level.

Fig. S5. Atomic distances between metal atoms in the OEC. The distances in the A- and B-monomers are depicted for LowDose-1 (at 0.03 MGy), LowDose-2 (at 0.12 MGy), and Native_0.43MGy (3WU2)[1] in red, blue, and green, respectively. Error bars are ± 0.1 Å.

Fig. S6. Atomic distances around the oxo-bridging oxygen atoms of the OEC for (a) O1, (b) O2, (c) O3, (d) O4, and (e) O5. The two A-monomers and two B-monomers in the LowDose-1 (at 0.03 MGy), LowDose-2 (at 0.12 MGy) structures are depicted in red, blue, orange, and cyan, respectively. Error bars are ± 0.1 Å.

Fig. S1 Tanaka et al.

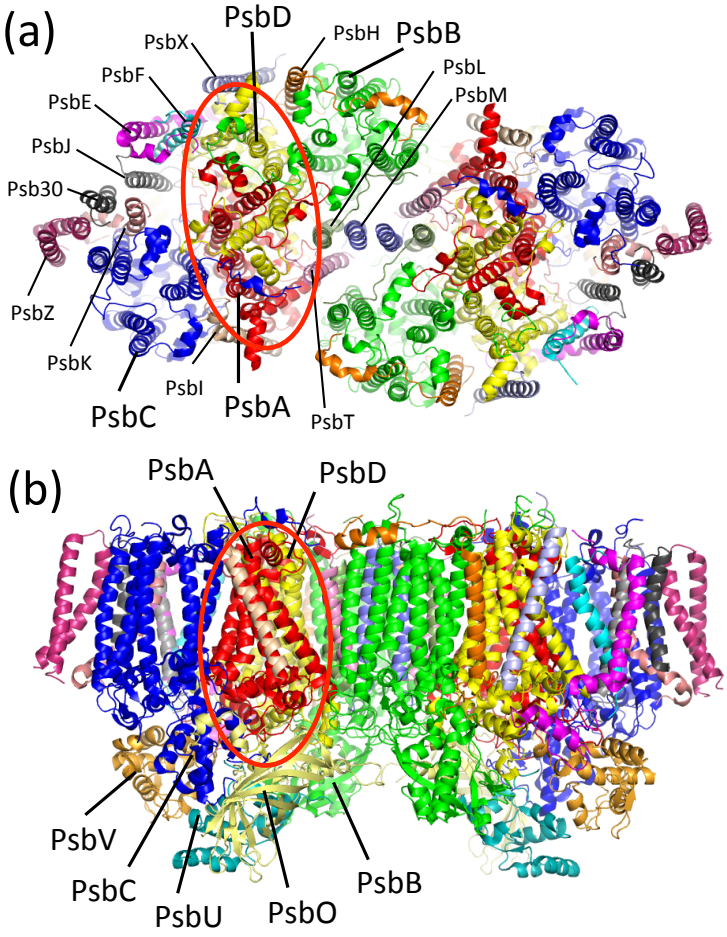

Fig. S2 Tanaka et al.

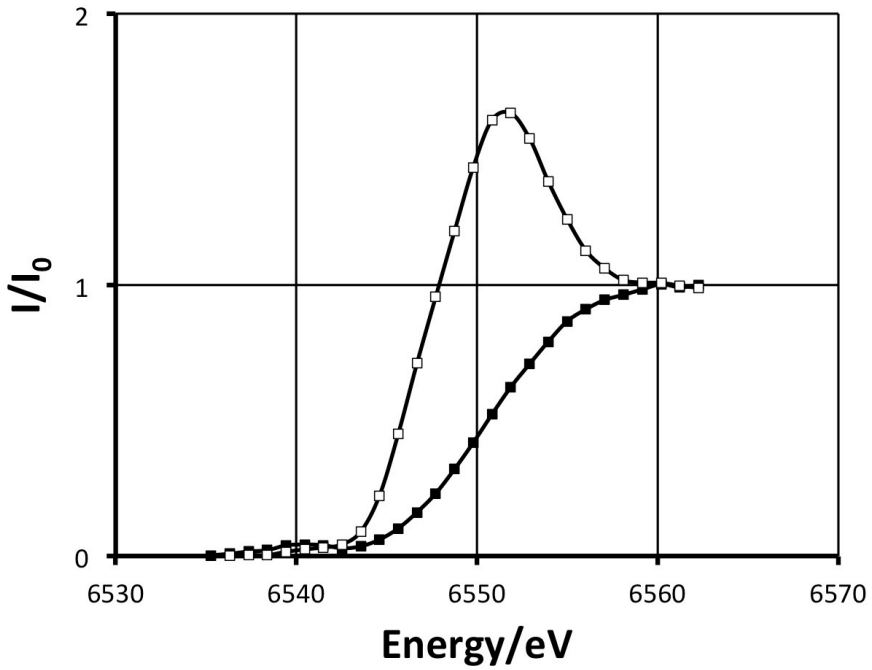

Fig. S3 Tanaka et al.

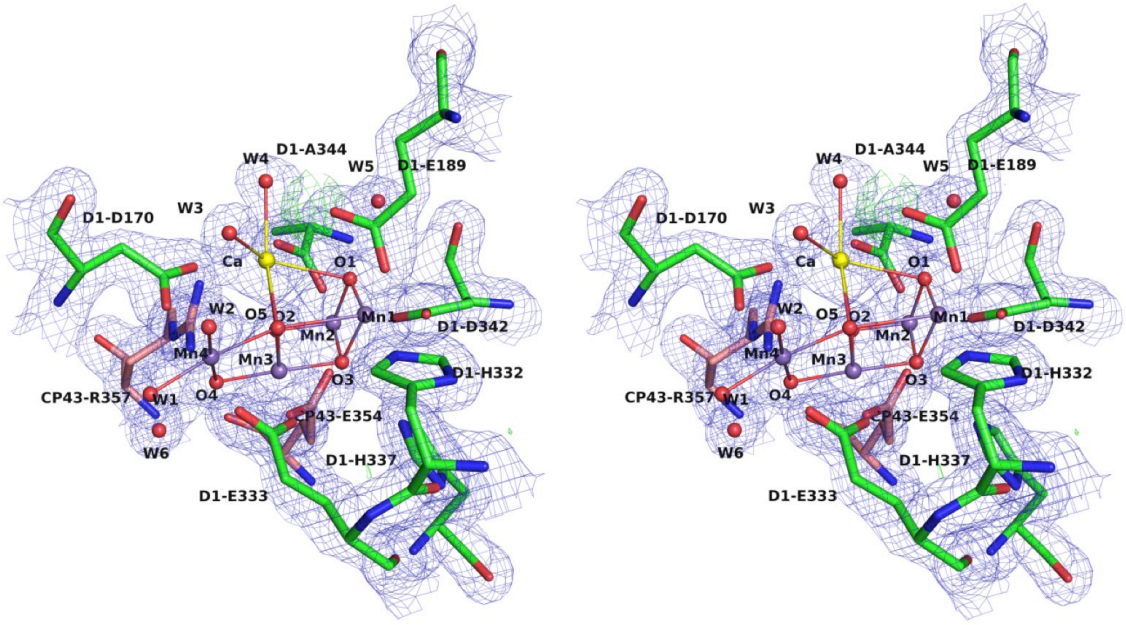

Fig. S4(a) Tanaka et al.

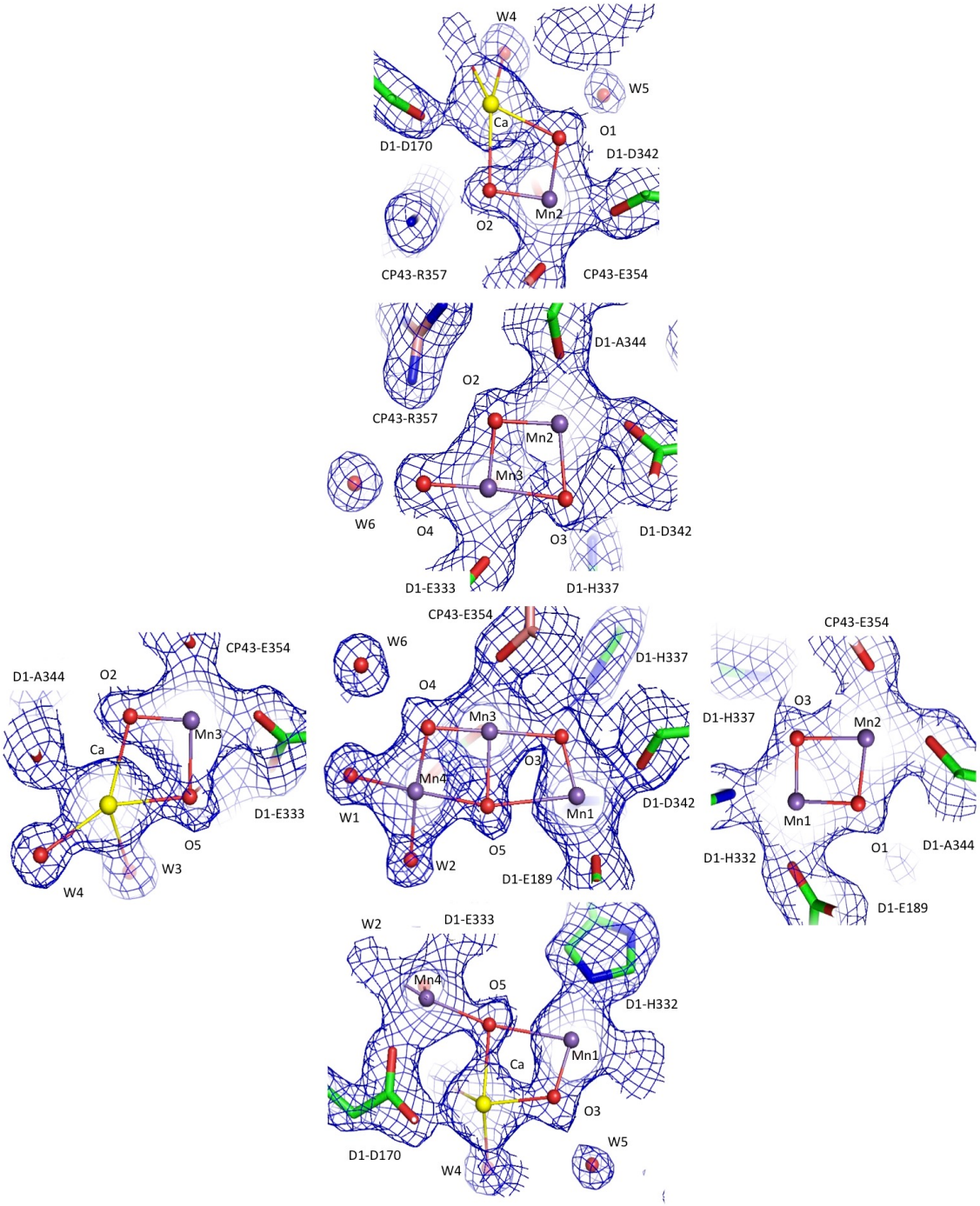

Fig. S4(b) Tanaka et al.

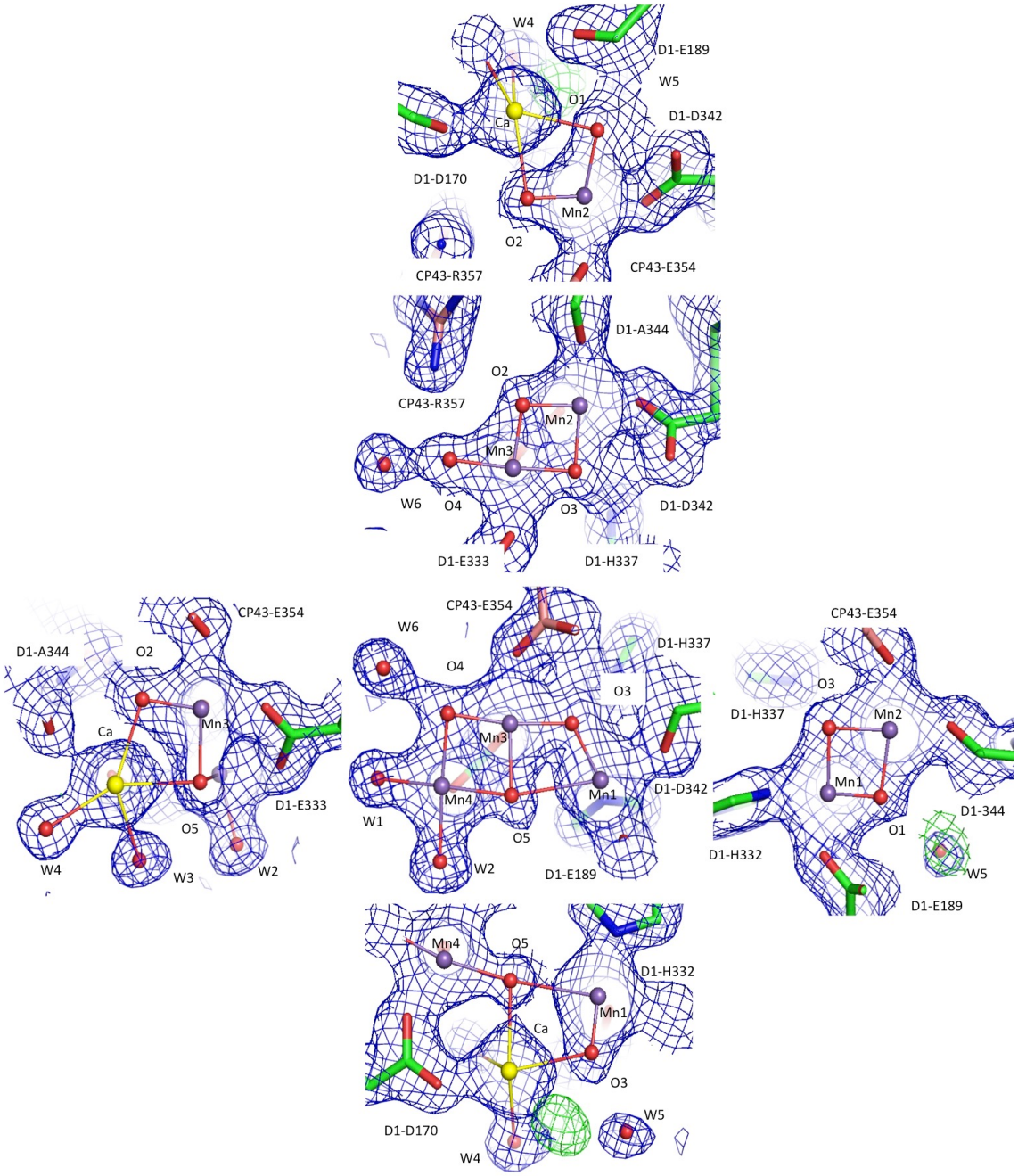

Fig. S5 Tanaka et al.

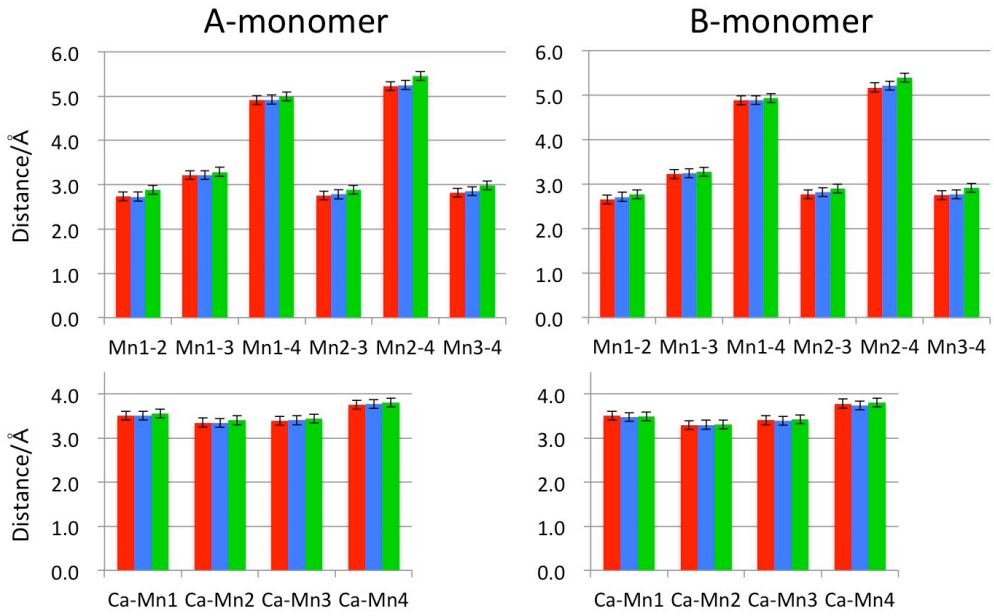

Fig. S6 Tanaka et al.

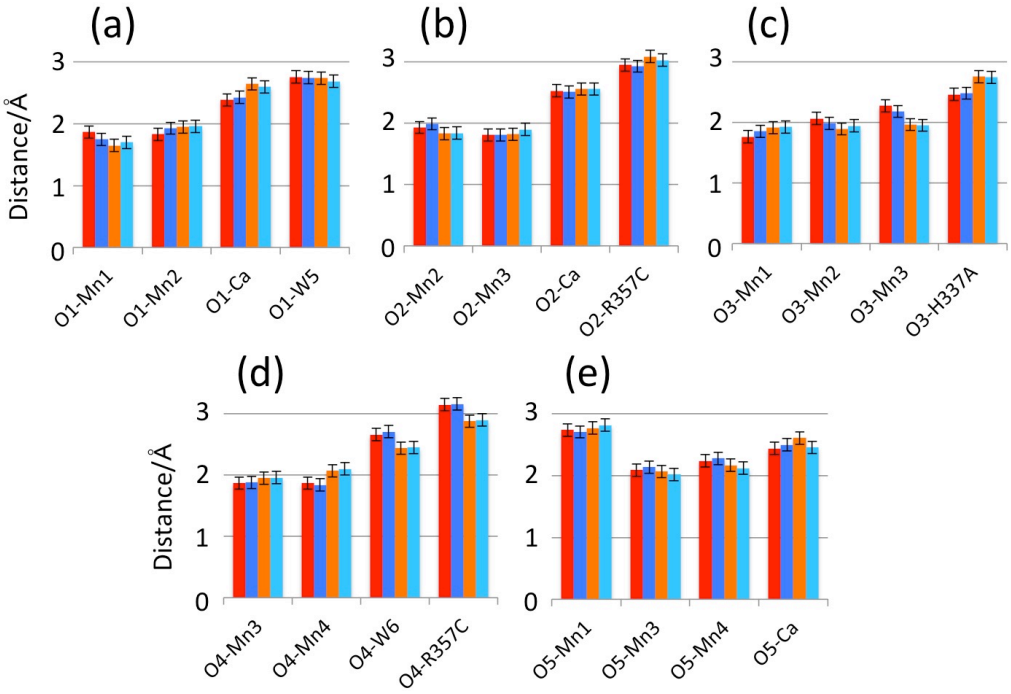

References

(1) Umena, Y.; Kawakami, K.; Shen, J.-R.; Kamiya, N. *Nature* **2011**, *473*, 55-60.

(2) Suga, M.; Akita, F.; Hirata, K.; Ueno, G.; Murakami, H.; Nakajima, Y.; Shimizu, T.; Yamashita, K.; Yamamoto, M.; Ago, H.; Shen, J.-R. *Nature* **2015**, *517*, 99-103.

(3) Kabsch, W. *J. Appl. Cryst.* **1993**, *26*, 795-800.

(4) Evans, P. R. *Acta Crystallogr.* **2006**, *D62*, 72-82.

(5) Murray, J. W.; Garman, E. F.; Ravelli, B. G. *J. Appl. Cryst*. **2004**, *37*, 513-522.

(6) Yano, J.; Kern, J.; Irrgang, K. D.; Latimer, M. J.; Bergmann, U. Glatzel, P., Pushkar, Y., Biesiadka, J., Loll, B., Sauer, K., Messinger, J.; Zouni, A.; Yachandra, V. K. *Proc. Natl. Acad. Sci. USA* **2005**, *102*, 12047-12052.

(7) Diederichs, K.; Karplus, P. A. *Acta Crystallogr*. **2013**, *D69*, 1215-1222.

(8) Vagin, A.; Teplyakov, A. *J. Appl. Cryst*. **1997**, *30*, 1022-1025.

(9) Murshudov, G. N.; Vagin, A. A.; Dodson, E. J. *Acta Crystallogr.* **1997**, *D53*, 240-255.

(10) Emsley, P.; Cowtan, K. *Acta Crystallogr*. **2004**, *D60*, 2126-2132.

(11) Brünger, A. T.; Adams, P. D.; Clore, G. M.; DeLano, W. L.; Gros, P.; Grosse-Kunstleve, R. W.; Jiang, J.-S.; Kuszewski, J.; Nilges, M.; Pannu, N. S.; Read, R. J.; Rice, L. M.; Simonson, T.; Warren, G. L. *Acta Crystallogr*. **1998**, *D54*, 905-921.

(12) DeLano, W. L. *The PyMOL Molecular Graphics System on World Wide Web http://www.pymol.org*.

(13) Cruickshank, D. W. J. *Acta Crystallogr*. **1999**, *D55*, 583-601.